Locating far-field impulsive sound sources in air by triangulation

Brian G. Ferguson, Lionel G. Criswick and Kam W. Lo

Citation: The Journal of the Acoustical Society of America **111**, 104 (2002); doi: 10.1121/1.1402618
View online: https://doi.org/10.1121/1.1402618
View Table of Contents: https://asa.scitation.org/toc/jas/111/1
Published by the Acoustical Society of America

Locating far-field impulsive sound sources in air by triangulation

Brian G. Ferguson, Lionel G. Criswick, and Kam W. Lo
Defence Science and Technology Organisation, P.O. Box 44, Pyrmont, NSW 2009, Australia

(Received 14 February 2000; revised 17 July 2001; accepted 19 July 2001)

The firing of a gun generates an acoustic impulse that propagates radially outwards from the source. Acoustic gun-ranging systems estimate the source position by measuring the relative time of arrival of the impulse at a number of spatially distributed acoustic sensors. The sound-ranging problem is revisited here using improved time-delay estimation methods to refine the source position estimates. The time difference for the acoustic wavefront to arrive at two spatially separated sensors is estimated by cross correlating the digitized outputs of the sensors. The time-delay estimate is used to calculate the source bearing, and the source position is cross fixed by triangulation using the bearings from two widely separated receiving nodes. The variability in the bearing and position estimates is quantified by processing acoustic sensor data recorded during field experiments for a variety of impulsive sound sources: artillery guns, mortars, and grenades. Imperfect knowledge of the *effective* speed of sound travel results in bias errors in the source bearing estimates, which are found to depend on the orientation of the sensor pair axis with respect to the source direction. Combining the time-delay estimates from two orthogonal pairs of sensors reduces these bias errors.
 [DOI: 10.1121/1.1402618]

PACS numbers: 43.28.Tc, 43.60.Gk [LCS]

I. INTRODUCTION

Historically, the military has viewed the accurate location and engagement of enemy indirect weapon systems as a vital factor on the battlefield. Sound ranging, which was first employed in World War 1, is the procedure used to locate guns and mortars by calculations based on the relative time of arrival of the sound impulse at several accurately located microphones. The time of arrival (travel time) depends on the local sound speed at each point along the acoustic propagation path from the source to the sensor. The relative time of arrival (commonly referred to as the differential time of arrival or simply, the time delay) is the difference in the times of arrival at two separate sensor positions. Passive ranging systems based on time-delay measurements at spatially distributed sensors assume isospeed sound propagation conditions when estimating the position of the source. Changing meteorological conditions lead to changing sound propagation conditions that can affect the accuracy of the source position estimates.

Although the location of artillery fire using acoustic means has traditionally been of military interest, it is the accuracy to which these sources of impulsive sound can be located that is of scientific interest.[1] The principles of sound ranging have not changed with time, and manually operated gun-ranging systems in the past have been limited by the magnitude of the error in the time-delay measurements, variously reported to be between 1 and 3 ms.[2,3] These historical systems employed an indirect method for time-delay estimation. First, each trace showing the variation of a sensor output with time is manually inspected for a ''break'' corresponding to the waveform of a gun-firing transient. Then, the beginning of the transient's waveform is taken as the time of arrival of the transient at the sensor. Finally, the time delay for a pair of sensors is calculated by taking the difference in the times of arrival of the transient at the two sensors. Errors arise because the time of the ''beginning'' of the transient tends to be subjective, especially in windy conditions when flow-induced noise at the sensor results in a low signal-to-noise ratio. The error in the time-delay estimate is equal to the sum of the errors in determining the two times of arrival.

In this paper, digital acoustic signal-processing techniques are used to reduce the time-delay measurement errors of traditional gun-ranging systems by an order of magnitude. The time delay for a pair of sensors is calculated automatically by cross correlating the outputs of the two sensors and then finding the time lag of the peak in the cross correlogram. The time-delay estimate obtained using this method can be interpreted as the time shift required for alignment of the transient waveforms received by the two sensors. An advantage of the cross-correlation method is that the time delay is measured directly, thus eliminating the errors associated with the indirect method. Also, the spatial correlation function of the flow-induced noise decreases with distance so that the effect of wind noise on the cross correlogram decreases as the sensor separation distance is increased; increasing the integration time also reduces the effect of wind noise. When the system errors are sufficiently small, the accuracy of the source position estimate depends on the wavefront angle-of-arrival variability for acoustic propagation in the atmosphere.

II. PASSIVE SOUND RANGING BY TRIANGULATION

The passive ranging of an acoustic source in the *near* field relies on measuring the curvature of the wavefront at the receiving array. For instance, knowing the sensor-separation distances and the isospeed of sound propagation in the medium, a three-element linear array can be used to estimate the range and bearing of the source by measuring the time delay between the center sensor and each of the other two sensors.[4–8] The radius of curvature of the wavefront is equal to the source range. For a source in the *far*

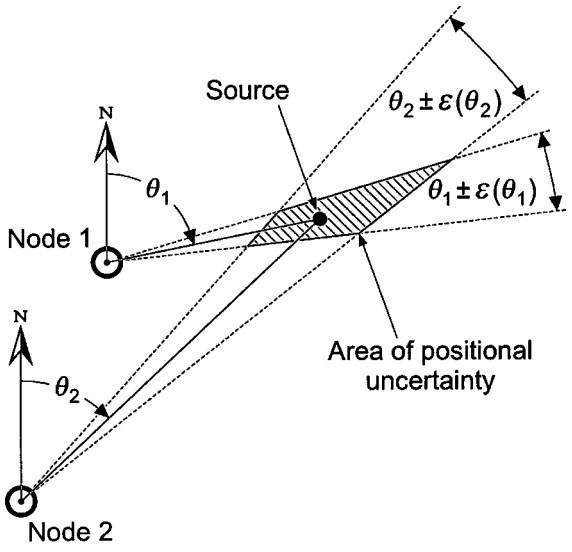

FIG. 1. Principle of triangulation using two widely separated nodes. Variability in the bearing estimates leads to an area of positional uncertainty within which the source lies.

field, however, the wavefront arriving at a receiving node of closely spaced sensors is planar, so only the bearing can be estimated. In this case, a range estimate is derived by triangulation using the bearing estimates from multiple widely separated nodes whose positions are accurately known. The required processing to determine the optimal position estimate (in the presence of bearing measurement errors) using three or more nodes has been described elsewhere.[9] This paper considers triangulation using two nodes.

Figure 1 shows the principle of triangulation using two nodes. The source and the two nodes, labeled 1 and 2, are located on the $x-y$ plane at coordinates (x_s, y_s), (x_1, y_1), and (x_2, y_2), respectively, with the y axis pointing towards the north. The bearing lines from the two nodes intersect to determine a unique source location. Assuming line-of-sight propagation, the source position is given by

$$x_s = (y_s - y_1)\tan\theta_1 + x_1, \tag{1}$$

$$y_s = \frac{x_2 - x_1 + y_1 \tan\theta_1 - y_2 \tan\theta_2}{\tan\theta_1 - \tan\theta_2}, \tag{2}$$

where θ_n is the source bearing measured relative to the y axis at node n $(n=1,2)$, that is, with respect to north. The positional uncertainty of the source, represented by the shaded area in Fig. 1, is determined by the uncertainties, $\varepsilon(\theta_1)$ and $\varepsilon(\theta_2)$, in the source bearings, θ_1 and θ_2, respectively.

Figure 2 shows the sensor configuration of each node used in this paper. There are three sensors, labeled 1, 2, and 3. The coordinates of sensor 1 define the position of the node. Sensors 2 and 3 are located at a distance d (25 m) from sensor 1 in the north and east directions, respectively. Sensors 1 and 2 constitute the north–south (NS) sensor pair that is orthogonal to the east–west (EW) sensor pair consisting of sensors 1 and 3. The source bearing can be estimated using either pair of sensors or both.

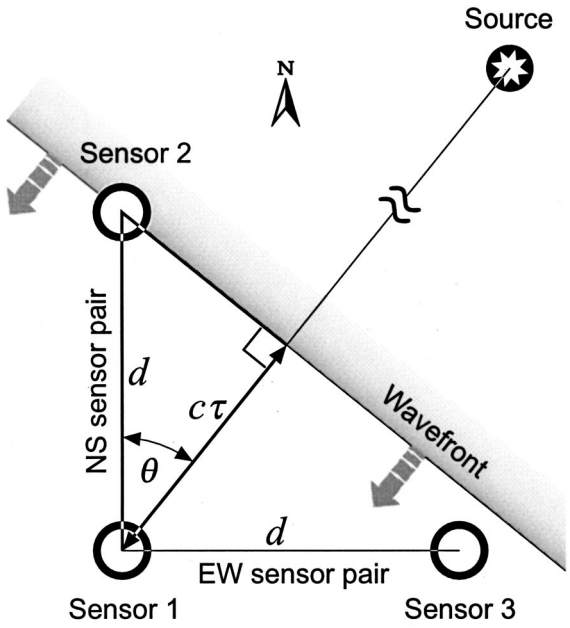

$$\cos\theta = \frac{c\tau}{d}$$

FIG. 2. Sensor configuration of each node. The source bearing is estimated here using the NS sensor pair—the product of the sound propagation speed c and the differential time of arrival τ divided by the sensor spacing d give the cosine of the relative bearing θ.

An estimate of the source bearing with respect to the NS sensor pair axis (referred to as the NS source bearing) is given by

$$\theta_{\mathrm{NS}} = \cos^{-1}(c\tau_{12}/d), \tag{3}$$

where c is the speed of sound propagation in air (typically 340 m/s), and τ_{12} is the time delay between sensors 1 and 2. The source bearing with respect to the EW sensor pair axis (referred to as the EW source bearing), θ_{EW}, is estimated using the same expression but with τ_{12} replaced by τ_{13}, which is the time delay between sensors 1 and 3. The NS bearing can also be estimated by using the time delays from both pairs of sensors, which are orthogonal to each other

$$\theta_{\mathrm{NS}} = \tan^{-1}(\tau_{13}/\tau_{12}). \tag{4}$$

III. FIELD EXPERIMENT

A field experiment is designed to quantify the errors of the triangulation method for the passive ranging of distant impulsive sound sources in the atmosphere. Figure 3 shows (to scale) the surveyed positions of the source (a 105-mm artillery gun) and the receiving nodes. A grid square denotes an area of 1 km by 1 km. The ground-truth (survey) data are shown for the bearing and distance of the source with respect to each of the nodes, and for the internodal distance. The bearings are measured with respect to Grid North (GN).

When the gun fires, an acoustic transient signal propagates radially outwards from the source. The curvature of the spherical wavefront decreases with range and, when it arrives at each node in the far field, the wavefront is considered

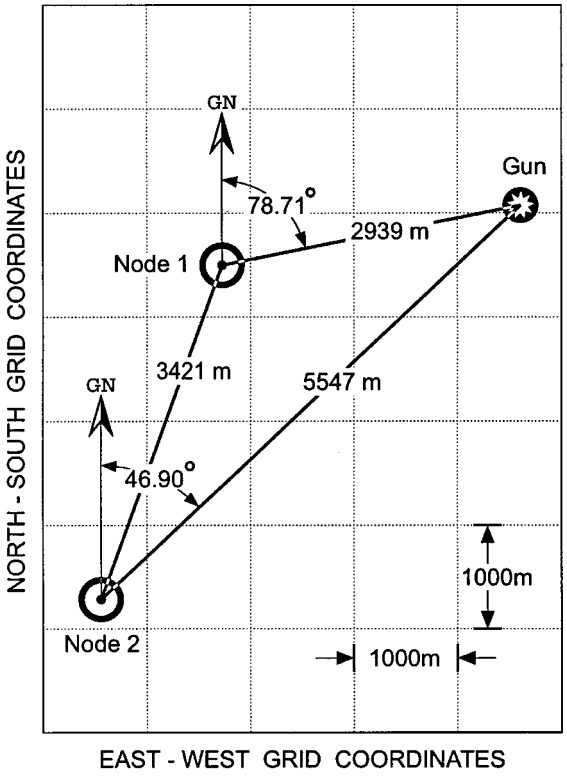

FIG. 3. Geometry of the field experiment. The distance from the source to each node and the distance between nodes are determined from the surveyed positions of the acoustic source (gun) and receiving nodes. The bearing of the source from each node is measured with respect to Grid North (GN).

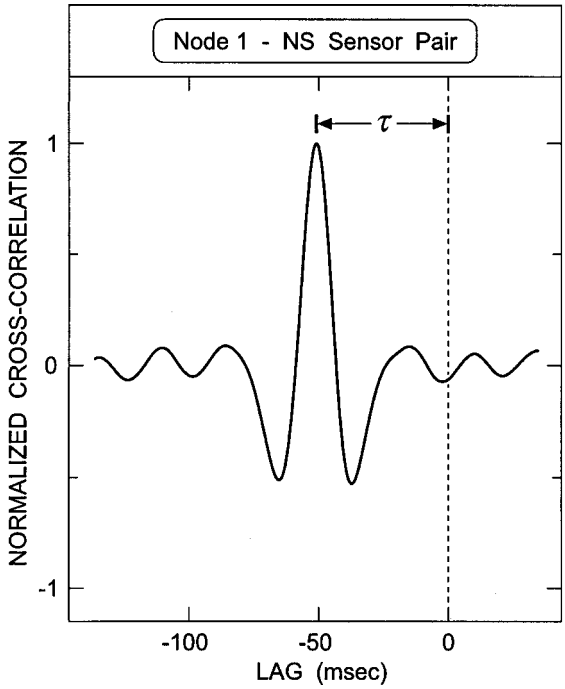

FIG. 4. Typical cross-correlation function of the gun-firing sound received by the NS sensor pair at node 1. The estimate of the differential time of arrival is given by the time lag τ at which the cross-correlation function attains its maximum value.

to be planar. Each of the sensor outputs is sampled at a rate of 20 000 times per second. The outputs of sensors 2 and 3 are each cross correlated with the output of sensor 1. The cross correlation is implemented in the frequency domain using a rectangular window function between 5 and 200 Hz, where most of the signal energy is contained. The integration or observation time is 0.2 s, which is short enough to ensure only one firing event occurs during the observation interval and yet much longer than the correlation time of noise. The signal-to-noise ratio at each sensor output exceeds 45 dB. Figure 4 shows a typical cross correlogram of the gun-firing sound received by the NS sensor pair at node 1 during the field experiment. The peak in the cross correlogram is well defined and its lag position gives an accurate estimate of the time delay between the two sensors. When the atmosphere is calm, the time-delay estimation accuracy is determined by the sampling period (0.05 ms), since the product of signal-to-noise ratio, integration time, and bandwidth is large. This represents an order of magnitude improvement in the time-delay measurement accuracy offered by early operational gun-ranging systems (quoted to be between 1 and 3 ms[2,3]). However, in practice, the time-delay estimation performance of any acoustic system depends strongly on atmospheric conditions. In the present experiment, the *minimum* standard deviation of the time delay estimates is 0.1 ms (observed for a gun-firing serial consisting of 22 events). For a time-delay error of 0.1 ms, the bearing estimate error using a single sensor pair is about 0.08° when the source direction is broadside to the sensor pair axis.

During the course of the field experiment, the gun is fired intermittently 206 times over a 20-h time period with the time intervals between firing serials being irregular. The source position of each firing event (gun primary) is computed by triangulation using the bearing estimates from nodes 1 and 2. (Note: Gun-ranging terminology refers to the firing of a shell as the ''primary'' and the bursting of the shell at the end of its trajectory as the ''secondary.'') Figure 5 shows the estimated source positions for all 206 firing events using the bearing estimates from the NS sensor pairs. Each grid square represents an area of 100 m by 100 m. Each white-filled circle represents a source position estimate. A black-filled square and a black-filled circle represent (respectively), the median and mean position estimates of all 206 events. The actual position (denoted by a black-filled triangle) corresponds to the surveyed position of the gun. The distance between the actual position and the *median* position estimate is 15 m, which is small considering that the gun is about 3 km from node 1 and 5.5 km from node 2. The distance between the actual position and the *mean* position is 25 m. The error covariance matrix is computed using all 206 position estimates. The result is then used to calculate the 1.5-sigma error ellipse, which is shown in Fig. 5 centered on the mean position estimate. About 74% of the source position estimates lie within this error ellipse. Due to the source-sensor node geometry, the spatial distribution of the position estimates (or error ellipse) is skewed towards the north of east, which is consistent with the direction of elongation of the positional uncertainty area shown in Fig. 1. Placing a third node to the south of the source would significantly reduce this elongation of the positional uncertainty area (that is, the error ellipse would appear more circular).

The accuracy of the source position estimates is deter-

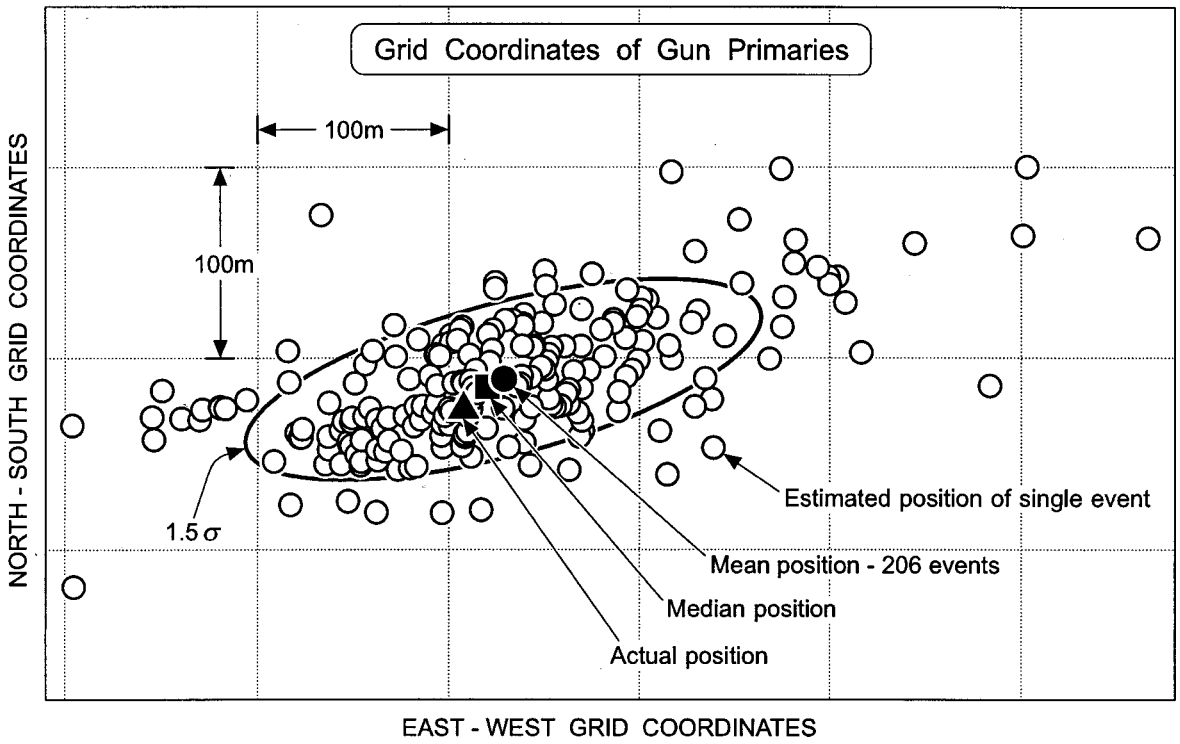

FIG. 5. Estimated grid coordinates for 206 gun-firing events and the 1.5-sigma error ellipse centered at the mean position estimate.

mined by the accuracy of the source bearing estimates. The source bearing error is equal to the difference between the bearing estimate (acoustic bearing) and the actual (surveyed) bearing of the source. Figures 6 and 7 show, for nodes 1 and 2, respectively, (a) the error in the (EW) source bearing estimated using the EW sensor pair and (b) the error in the (NS) source bearing estimated using both sensor pairs versus the error in the (NS) source bearing estimated using the NS sensor pair. The mean errors are shown in the figures as black-filled circles. It can be observed from Fig. 6(a) that for node 1, the variance of the source bearing errors using the EW sensor pair is larger than that using the NS sensor pair. Also, the source bearing estimates are biased in all cases, and the bias is larger when using the EW sensor pair.

The difference in bearing estimation performance using different sensor pairs is attributed to the direction of the source relative to the orientation of the sensor pair axis coupled with various factors such as time-delay estimation errors, imperfect knowledge of the speed of sound travel, and refraction of the acoustic wavefronts. The Appendix provides a brief statistical analysis of the bearing error due to each of these factors when using either a single pair of sensors or two orthogonal pairs of sensors. With a single pair of sensors, the bias and the variance of the bearing estimate always increase (regardless of the cause of the error) as the source direction tends to either of the end-fire directions of the sensor pair axis (that is, source bearing approaches 0° or 180°). Assuming the errors are constant, Fig. 8 shows the predicted bearing error as a function of the actual source bearing for (1) an error of 5 m/s in the assumed sound speed (340 m/s); (2) an apparent source elevation angle of 6° (rather than the assumed value of 0°) due to vertical refraction of the acoustic wavefronts; and (3) an error of 0.1 ms in the time-delay estimate. The bearing error is smallest when the source direction coincides with the broadside direction of the sensor pair axis (source bearing equals 90°). The bearing error increases rapidly as the source direction approaches the end-fire direction (source bearing equals 0°). With two orthogonal pairs of sensors, the bearing accuracy is not affected by the error in the assumed sound speed. Also, the bearing estimate actually represents the azimuth angle estimate, thus, vertical refraction of the acoustic wavefronts does not cause any bearing error. Furthermore, the bearing accuracy will be independent of the actual source bearing if the errors in τ_{12} and τ_{13} are statistically independent, zero-mean, and with the same variance.

The results shown in Figs. 6 and 7 suggest that for the present experiment, the bearing estimates from the NS sensor pairs at nodes 1 and 2 will provide the most accurate source position estimate. Figures 9(a) and 9(b) show the cumulative probability distributions of the source bearing errors for all 206 firing events using the NS sensor pairs at nodes 1 and 2, respectively, while Fig. 9(c) shows the cumulative probability distribution of the resulting source position errors. [Note that the source position error is defined here as the *distance* between the position estimate and the actual (surveyed) position of the source.] Figure 10 compares the cumulative probability distributions of the source position errors for all 206 firing events using the NS sensor pairs, the EW sensor pairs, and both NS and EW sensor pairs at nodes 1 and 2. This figure confirms that for the present experiment, the NS sensor pairs provide the best gun-ranging results but those obtained using both NS and EW sensor pairs are comparable. Table I(a) lists the source bearing errors and source position errors using the NS sensor pairs for cumulative probabilities of 0.5, 0.75, and 0.9; for example, there is a 75% probability

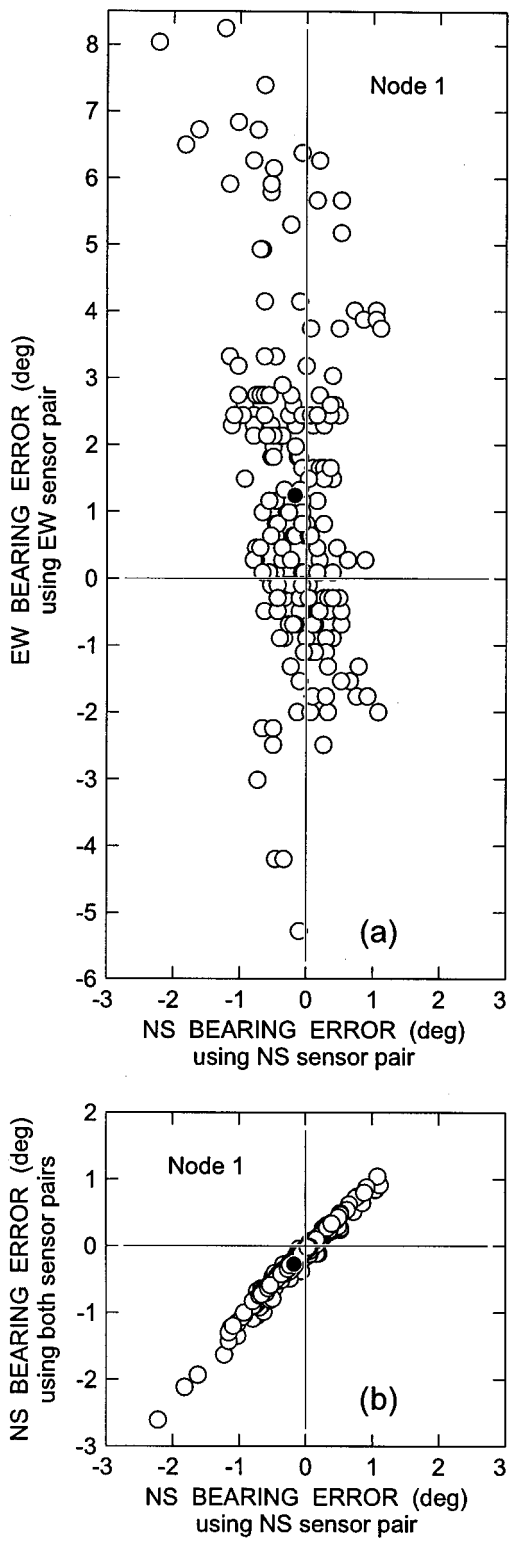

FIG. 6. For node 1: (a) Variation of the EW source bearing error using the EW sensor pair with the NS source bearing error using the NS sensor pair. (b) Variation of the NS source bearing error using both the NS and EW sensor pairs with the NS source bearing error using the NS sensor pair. The black-filled circle represents the mean bearing error.

that the source position error is less than 103 m. Tables I(b) and (c) list the corresponding results obtained using the EW sensor pairs and both NS and EW sensor pairs at the two nodes, respectively. The source position errors using the EW

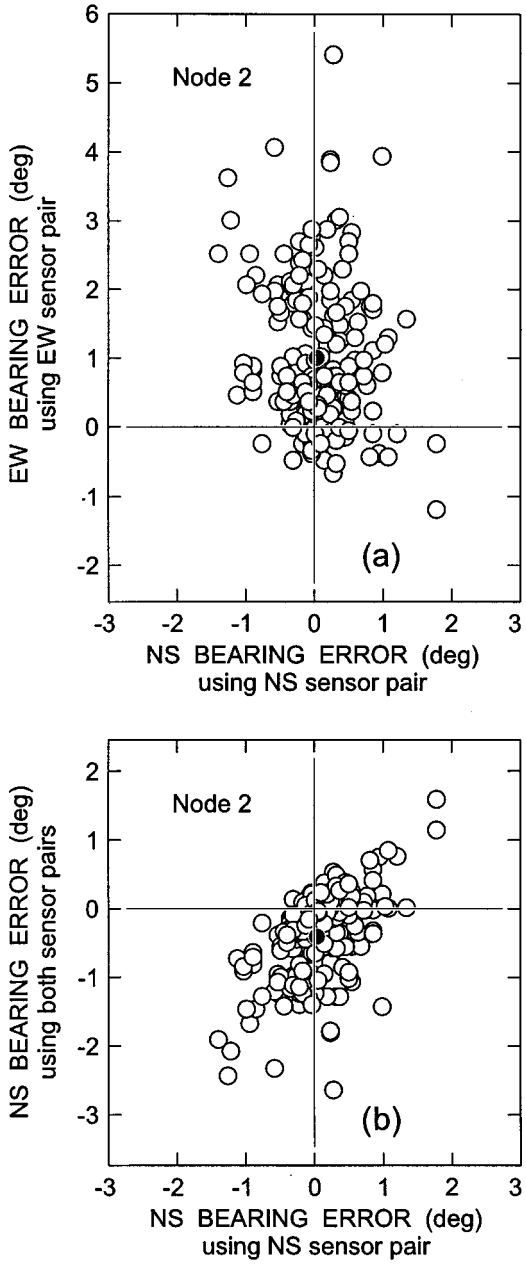

FIG. 7. For node 2: (a) Variation of the EW source bearing error using the EW sensor pair with the NS source bearing error using the NS sensor pair. (b) Variation of the NS source bearing error using both the NS and EW sensor pairs with the NS source bearing error using the NS sensor pair. The black-filled circle represents the mean bearing error.

sensor pairs are roughly double those using the NS sensor pairs.

IV. METEOROLOGICAL EFFECTS

A. Ground wind and temperature variations

Meteorological effects on sound propagation have been reported for many years in the literature.[10,11] The effect of wind must be considered in sound ranging together with temperature.[2] The travel of sound is superimposed on that of the wind whose effect is usually more important than that of temperature. In the present experiment, the (ground) temperature varied from 13° to 16 °C, which corresponds to a

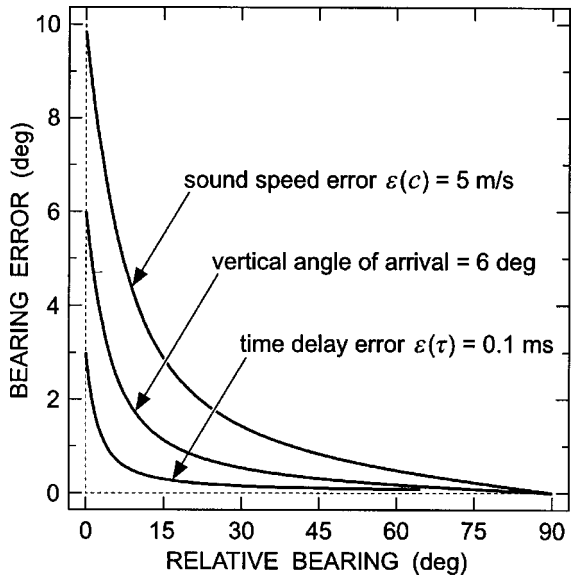

FIG. 8. Predicted bearing error as a function of the actual source bearing for (1) an error of 5 m/s in the assumed sound speed (340 m/s); (2) an apparent source elevation angle of 6° (rather than the assumed 0°); and (3) an error of 0.1 ms in the time-delay estimate. The bearing is measured with respect to the sensor pair axis.

sound-speed variation of 1.8 m/s, while the (ground) wind speed varied from 0 to 6 m/s over the 20-h period. The wind speed and direction, together with temperature, were logged every 2 min at node 1 *only*.

The effect of wind on sound-ranging system performance depends on the relative bearing of the source, that is, the direction of the source with respect to the orientation of the sensor pair axis. The speed of sound travel at node 1 (which was previously assumed constant at 340 m/s) is adjusted to include the effects of changes in wind velocity and temperature. Figure 11 shows a plot of the resulting EW source bearing error using the EW sensor pair against the NS source bearing error using the NS sensor pair at node 1 for each of the 206 firing events. Figure 12 shows the cumulative probability distributions of the source bearing errors using each of the sensor pairs (NS, EW) at node 1, with and without correction for the effects of wind- and temperature variations on the speed of sound travel. The difference in the source bearing errors using the NS sensor pair before and after the correction is found to be negligible. This is because the bearing estimate is insensitive to errors in the speed of sound travel when the source is near the broadside direction of the NS sensor pair. Comparing Fig. 11 with Fig. 6(a), the bias and variance of the source bearing errors using the EW sensor pair are reduced after correction for the effects of wind and temperature variations on the speed of sound travel; these reductions are represented by the shaded area in Fig. 12. However, the source bearing errors using the EW sensor pair are still larger (in a statistical sense) than those using the NS sensor pair after the correction. This is due to the fact that the source direction is near the end-fire direction of the EW sensor pair so that time-delay estimation errors and vertical refraction of the acoustic wavefronts have larger effects on the bearing accuracy of this sensor pair—see Fig. 8.

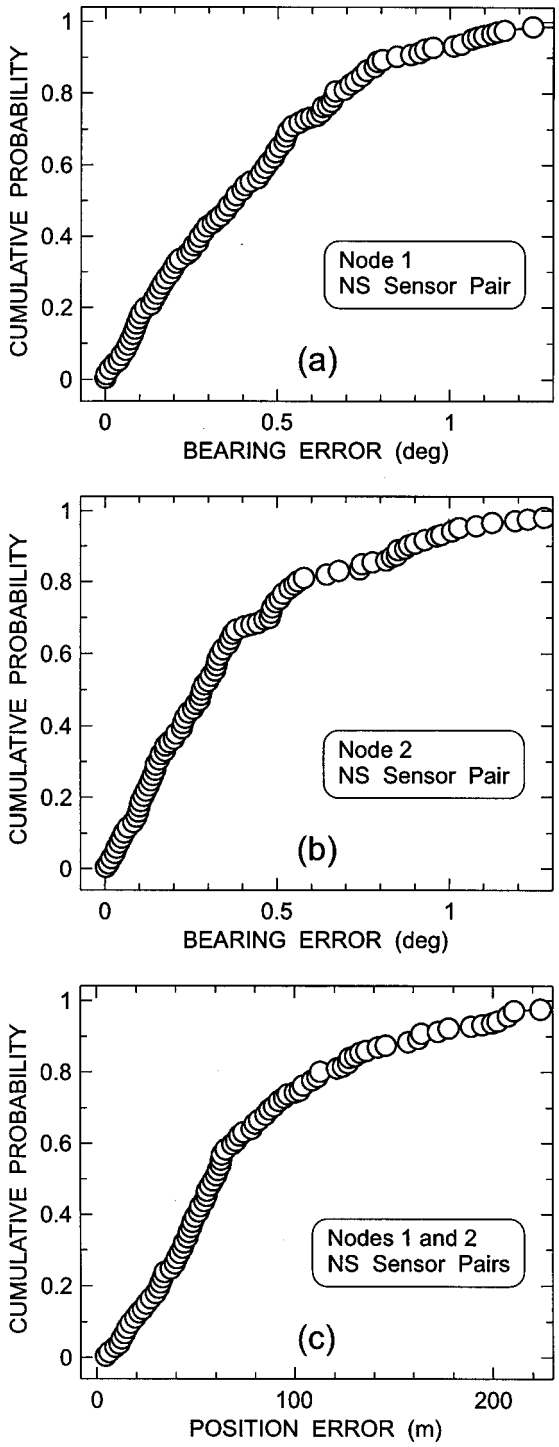

FIG. 9. (a) Cumulative probability distribution of the source bearing errors using the NS sensor pair at node 1. (b) Cumulative probability distribution of source bearing errors using the NS sensor pair at node 2. (c) Cumulative probability distribution of the source position errors using the NS sensor pairs at nodes 1 and 2.

B. Vertical refraction

The present source localization method assumes an isospeed sound propagation medium and hence straight-line propagation. However, the speed of sound propagation is dependent not only on ground wind and temperature, but also on conditions in the upper air. Knowledge of the vertical profiles of wind and temperature is required to determine the

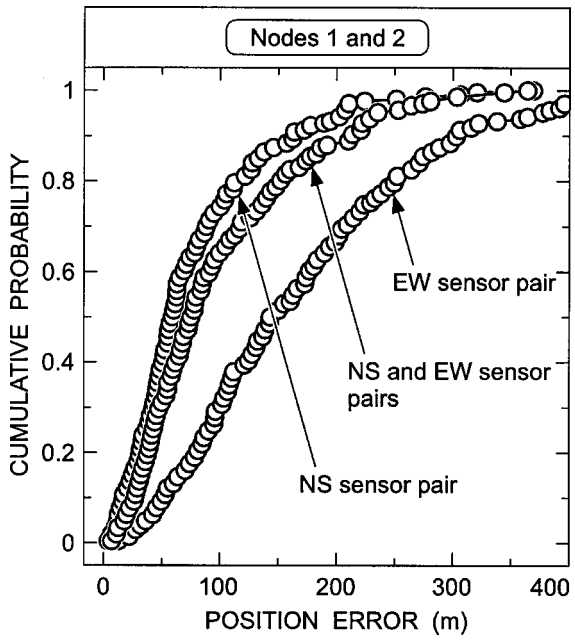

FIG. 10. Cumulative probability distributions of the source position errors using the NS sensor pairs, the EW sensor pairs, and both the NS and EW sensor pairs at nodes 1 and 2.

sound propagation path from the source to the sensor. Normally, with increasing height, there is a decrease in temperature and an increase in wind speed. These gradients of temperature and wind speed cause refraction of the wavefront in the vertical direction, and the acoustic wavefront arrives at the node with a finite elevation angle ϕ as depicted in Fig. 13. When the acoustic wavefront undergoes vertical refraction, it is the *apparent* bearing β (rather than the *actual* bearing θ) that is estimated by the NS (or EW) sensor pair. The cosine of the apparent bearing β (relative to the sensor pair axis) is equal to the product of the cosines of the azimuth angle θ (relative to the sensor pair axis) and elevation angle ϕ, that is, $\cos\beta=\cos\theta\cos\phi$. If the source is broadside to the sensor pair axis ($\theta=90°$), then the apparent bearing is equal to the azimuth angle ($\beta=\theta$) and is independent of ϕ, while at end-fire ($\theta=0°$) the apparent bearing is equal to the elevation angle ($\beta=\phi$). Thus, when using a single pair of sensors for bearing estimation, the effect of vertical refraction is minimal when the source direction is broadside to the sensor pair axis—see Fig. 8.

Ideally, knowledge of the apparent source elevation angle ϕ is required to compensate for the effect of vertical refraction of the acoustic wavefronts; otherwise, the source bearing estimates will be biased. An *effective* sound speed can be defined by $c_{\text{eff}}=c/\cos\phi$, which includes the effects of ground wind and temperature variations in the numerator (c) and the effect of vertical refraction in the denominator ($\cos\phi$). For a given sensor spacing d, the effective sound speed c_{eff} maps the time delay τ to the azimuth angle of the source θ, that is, $\cos\theta=c_{\text{eff}}\tau/d$.

The variability in the source bearing estimates caused by wavefront refraction effects can be observed in the present experiment by dividing the 206 firing events into nine groups; each group corresponds to a firing serial that lasted from 10 to 90 min. For each group of firing events (firing serial), the mean and standard deviation of the bearing estimates from each sensor pair at node 1 are calculated, and the results for the NS and EW sensor pairs are shown (respectively), in Fig. 14(a.1) for β_{NS} and Fig. 14(c.1) for β_{EW}. Here, a circle denotes the mean value and the error bars denote $\pm$ one standard deviation. Note that the bearing estimates (β_{NS}) from the NS sensor pair are measured with respect to Grid North and the bearing estimates (β_{EW}) from the EW sensor pair are measured with respect to Grid East. Similarly, the results for node 2 are shown in Fig. 14(a.2) for β_{NS} and Fig. 14(c.2) for β_{EW}. The bearing estimates from the NS (or EW) sensor pair are estimates of the apparent bearing β rather than the azimuth angle θ of the source. To estimate the azimuth angle θ of the source requires the use of both the EW and NS sensor pairs (see Appendix B 2). Figures 14(b.1) and 14(d.1) show for each firing serial the mean and standard deviation of the azimuth angle estimates (obtained using both sensor pairs at node 1) with respect to Grid

TABLE I. Values of the source bearing and position errors for specific values of cumulative probability (0.5, 0.75, and 0.9) using (a) the NS sensor pairs; (b) the EW sensor pairs; and (c) both the NS and EW sensor pairs, at nodes 1 and 2.

(a) North - South Sensor Pairs

Cumulative Probability	Bearing Error (°) Node 1	Bearing Error (°) Node 2	Position Error (m)
0.5	0.37	0.28	59
0.75	0.63	0.51	103
0.9	0.83	0.88	163

(b) East - West Sensor Pairs

Cumulative Probability	Bearing Error (°) Node 1	Bearing Error (°) Node 2	Position Error (m)
0.5	1.59	0.68	143
0.75	2.63	1.74	226
0.9	4.50	2.46	303

(c) Both NS and EW Sensor Pairs

Cumulative Probability	Azimuth Error (°) Node 1	Azimuth Error (°) Node 2	Position Error (m)
0.5	0.35	0.40	75
0.75	0.65	0.92	137
0.9	0.89	1.32	212

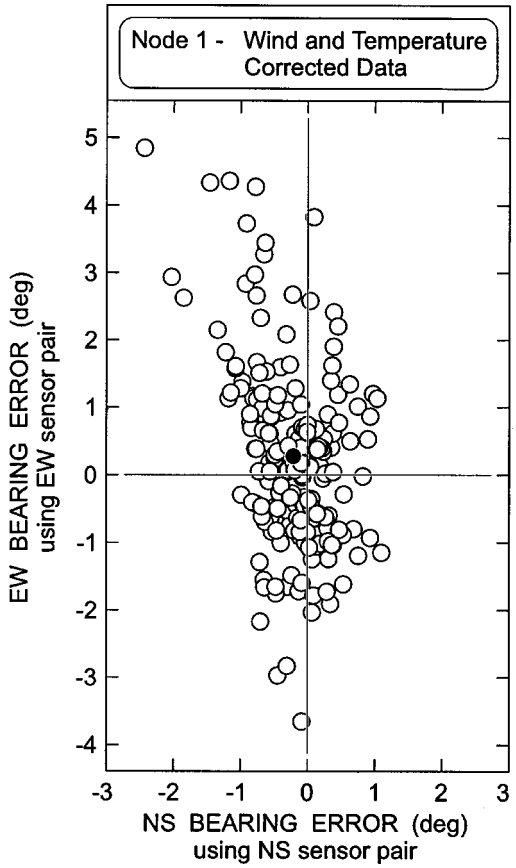

FIG. 11. For node 1: Variation with the NS source bearing error using the NS sensor pair of the EW source bearing error using the EW sensor pair, after correction for the effects of changes in wind velocity and temperature.

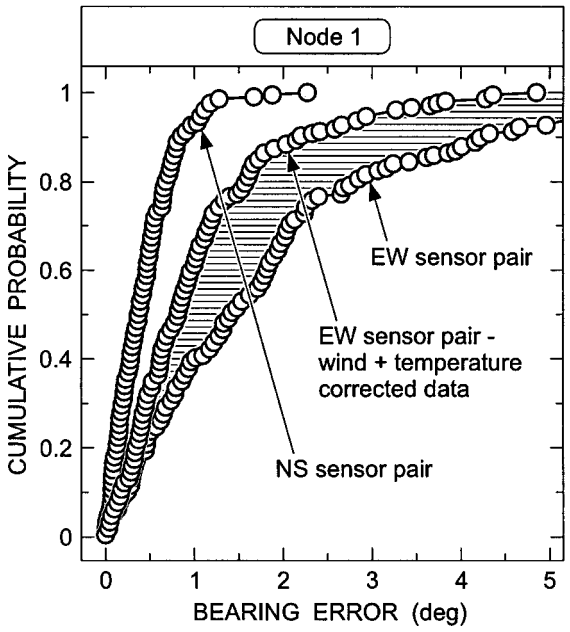

FIG. 12. Cumulative probability distributions of source bearing errors using the EW sensor pair at node 1, with and without correction for the effects of wind and temperature variations. The results for the NS sensor pair are also shown where the corrections for the effects of wind and temperature variations are negligible.

North and Grid East, respectively. The azimuth angle estimates with respect to Grid North θ_{NS} [see Fig. 14(b.1)] and Grid East θ_{EW} [see Fig. 14(d.1)] are complementary angles. Similarly, the results for node 2 are shown in Fig. 14(b.2) for θ_{NS} and Fig. 14(d.2) for θ_{EW}.

The biasing effect of *vertical* refraction on bearing estimation can be readily observed by comparing Fig. 14(c.1) for β_{EW} with Fig. 14(d.1) for θ_{EW}. The bias errors for β_{EW} are much larger than those for θ_{EW}. Vertical refraction of the acoustic wavefronts leads to β being a (positively) biased estimate of the actual bearing θ; the magnitude of the bias error is a maximum for the end-fire (0°) source direction and a minimum (zero) for the broadside (90°) source direction. The bias errors for β_{NS} [see Fig. 14(a.1)] are small because the source direction (78.7°) is near the broadside direction of the NS sensor pair axis. In comparison, the bias errors for β_{EW} [see Fig. 14(c.1)] are much larger because the source direction (11.3°) is near the end-fire direction of the EW sensor pair axis.

Figure 15 shows the corresponding results after correction for the effects of wind and temperature variations on the speed of sound travel. The remaining bias errors for the EW sensor pair after the correction [see Fig. 15(b) β_{EW}] are ascribed partly to the downward refraction of the wavefronts resulting from the prevailing vertical meteorological conditions (and partly to horizontal refraction as discussed in the next section).

C. Horizontal refraction

Horizontal refraction of the acoustic wavefronts shifts the azimuth angle θ of the source in a particular direction. For node 1, the bias errors in θ shown in Fig. 14(b.1) for θ_{NS} and Fig. 14(d.1) for θ_{EW} as deviations of the mean values from the actual value are attributed to *horizontal* refraction

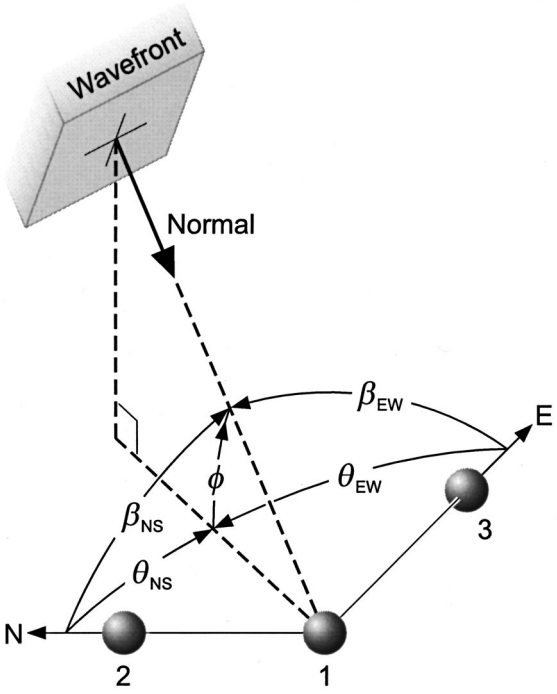

FIG. 13. An acoustic wavefront arrives at the sensor node with elevation angle ϕ due to vertical refraction; β and θ denote the respective apparent bearing and azimuth angles.

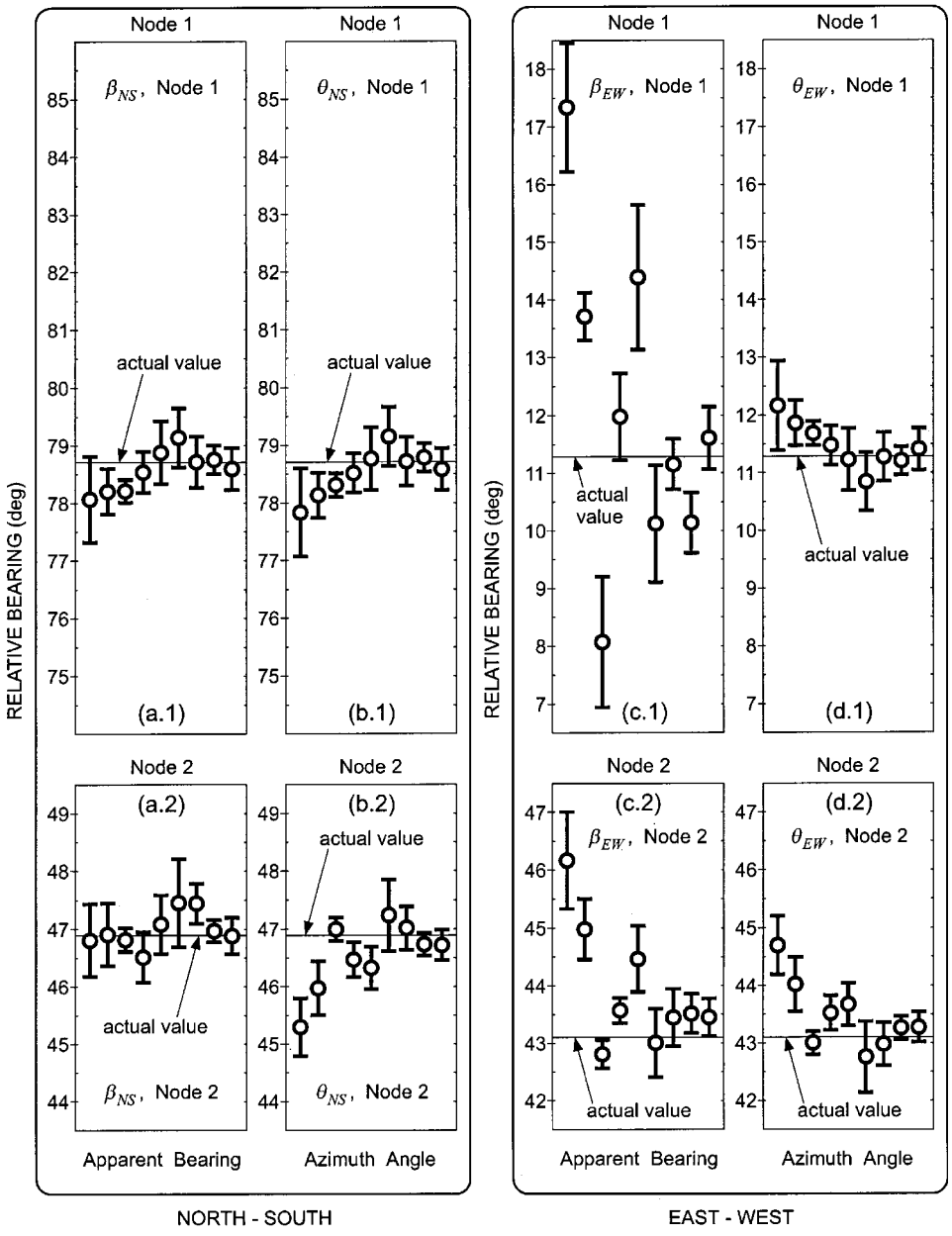

FIG. 14. Variability in the apparent bearing β and azimuth angle θ data at: Node 1—(a.1) β_{NS}; (b.1) θ_{NS}; (c.1) β_{EW}; (d.1) θ_{EW}; and Node 2—(a.2) β_{NS}; (b.2) θ_{NS}; (c.2) β_{EW}; (d.2) θ_{EW}.

of the acoustic wavefronts. Similar observations can be made for the node 2 results shown in Fig. 14(b.2) for θ_{NS} and Fig. 14(d.2) for θ_{EW}.

At node 2, the source is located at almost 45° with respect to the orthogonal axes of the sensor pairs, so the effects of wind/temperature variations and vertical refraction should be about the same for both sensor pairs. However, the bias errors of the bearing estimates from the NS sensor pair [see Fig. 14(a.2) β_{NS}] are smaller than those from the EW sensor pair [see Fig. 14(c.2) β_{EW}]. This unexpected result can be explained by the bias errors due to vertical and horizontal refraction compensating each other for the NS sensor pair. Such bias error compensation does not occur for the azimuth angle estimates from two orthogonal sensor pairs [see Fig. 14(b.2) θ_{NS}] because they are not affected by vertical refraction (only by horizontal refraction). It also explains why, for the present experiment, the source localization performance of the triangulation method is better when using the apparent bearings of the NS sensor pairs (β_{NS} from node 1 and β_{NS} for node 2) instead of the azimuth angles from both the NS and EW sensor pairs at the two nodes—compare Table I(a) with Table I(c).

V. OTHER OBSERVATIONS OF SOURCE BEARING VARIABILITY

Real data from two other field experiments are processed to extract information on the bearing variability of other impulsive sound sources: 155-mm guns, mortars, and grenades. Only a single node is deployed in these two ex-

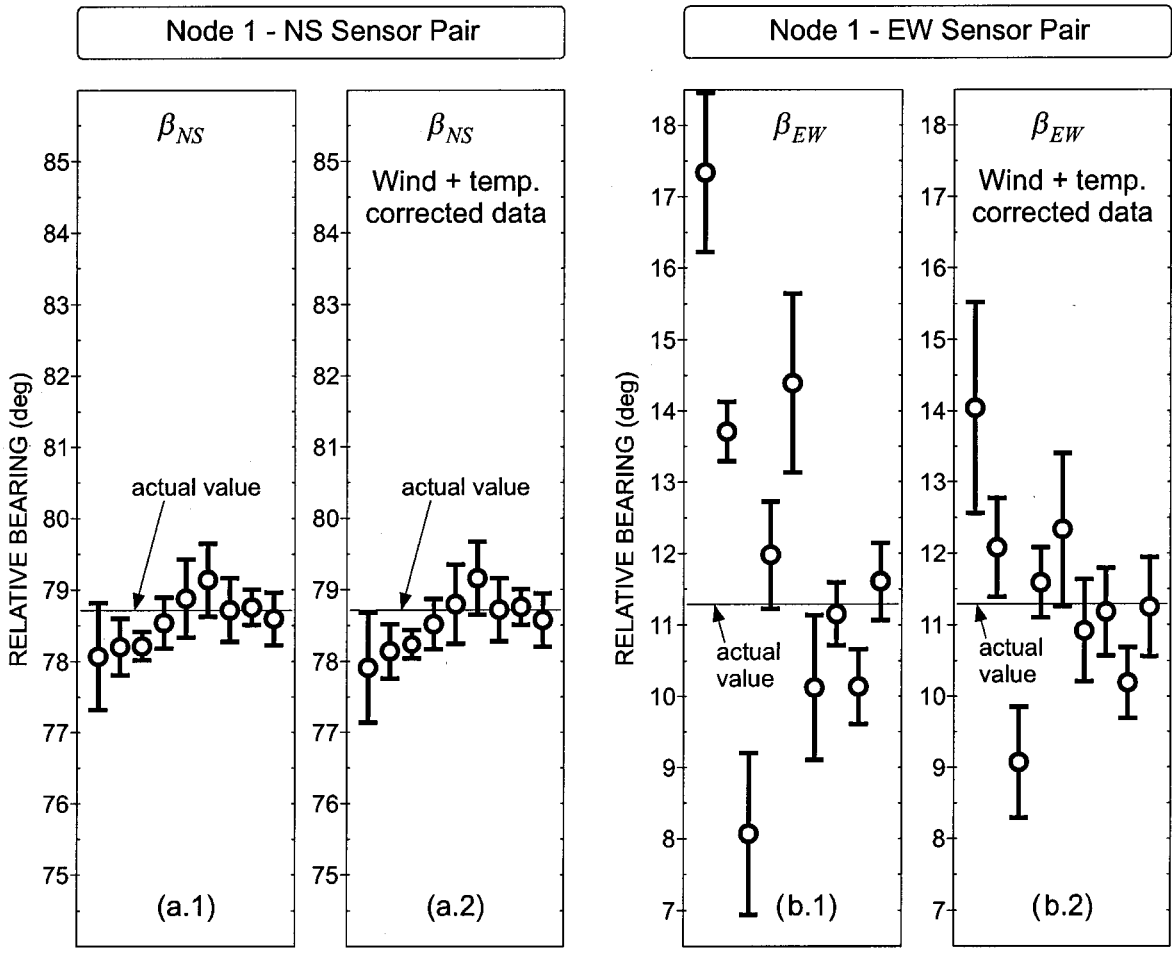

FIG. 15. For node 1: Variability in (a) the NS bearing (β_{NS}) data from the NS sensor pair and (b) the EW bearing (β_{EW}) data from the EW sensor pair *before* [(a.1), (b.1)] and *after* [(a.2), (b.2)] correction for the effects of wind and temperature variations.

periments, which were conducted on an opportunity basis. Accurate survey data for each source position and ground wind vector data are not available. The NS and EW sensor pairs are used, in turn, to estimate the (apparent) bearing of the source relative to the sensor pair axis.

The variability in the relative bearing estimates of the firing events is characterized using the mean and standard deviation, respectively, as measures of the central tendency and dispersion. For example, Fig. 16 shows the relative bearing observations of (155-mm) gunfire over two time periods of 62 min (period 1) and 17 min (period 2); there is a 58-min intermission between the gunfire serials. The estimated val-

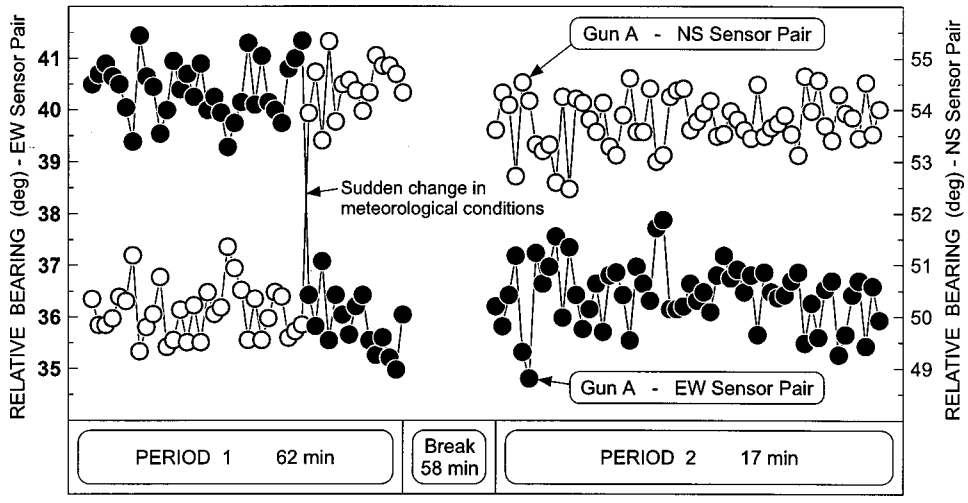

FIG. 16. Relative bearing data from the NS sensor pair and the EW sensor pair for a 155-mm gun (gun A) before, and after, a sudden change in the meteorological conditions.

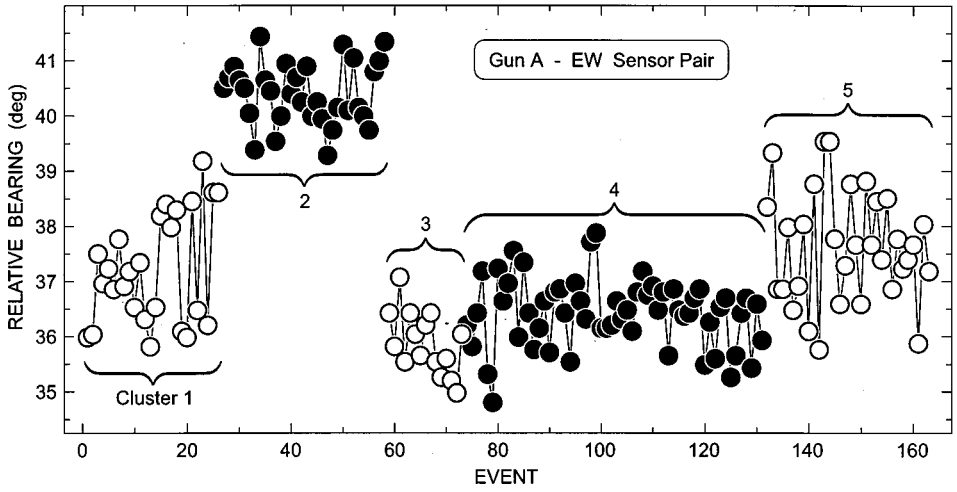

FIG. 17. Relative bearing data from the EW sensor pair for a 155-mm gun (gun A). The data are grouped as clusters, each cluster corresponding to a firing serial. Cluster 2 and 3 belong to the same firing serial, but are grouped separately due to the effect of a sudden change in meteorological conditions.

ues for the EW source bearing from the EW sensor pair are shown on the left-hand-side vertical axis (35–41°), and the estimated values for the NS source bearing from the NS sensor pair are shown on the right-hand-side vertical axis (49–55°). Initially, the variability in the bearing estimates resembles a random process and is attributed to the effects of time-delay estimation errors[8] and atmospheric turbulence.[12] Then, there is a discontinuity in the bearing estimates during period 1, which coincides with the arrival of a weather front and a sudden change in the meteorological conditions. The change in sound propagation conditions results in a systematic change of at least 4° in the source bearing estimates, which would have a significant impact on the source localization performance of the triangulation method. For the remainder of period 1, and for period 2, the variability in the bearing estimates again resembles a random process but with a different mean value. Random fluctuations in the atmosphere's wind and temperature fields produce random fluc-

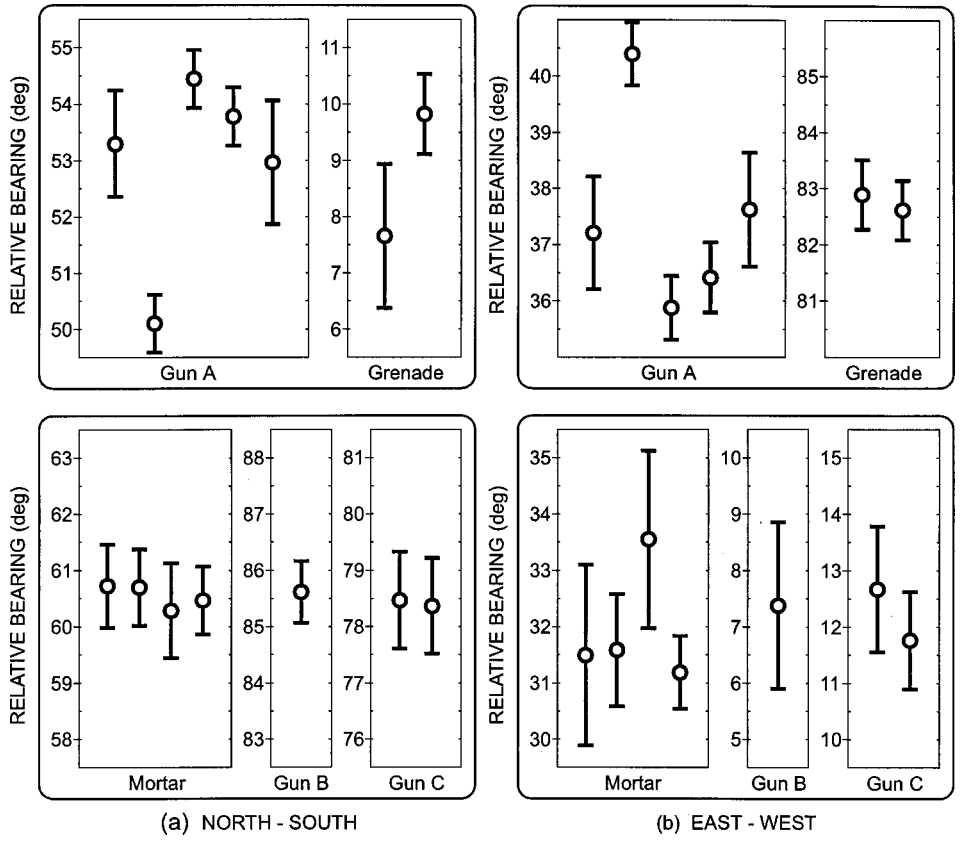

FIG. 18. Variability in the relative bearing data from (a) the NS sensor pair and (b) the EW sensor pair for all the sources studied during the other two field experiments. Each circle represents the mean value of the bearing data for a cluster (that is, a group of events corresponding to a firing serial) with the errors bars representing ± one standard deviation.

tuations in the intensity (acoustic scintillation) and orientation of the acoustic wavefronts (angle-of-arrival fluctuations) impinging on acoustic sensor arrays.[12]

In Fig. 16, the systematic change in the bearing estimates occurs over a short time period (minutes); however, changes are also observed to occur over longer time periods (hours to days). Figure 17 shows the EW source bearing estimates from the EW sensor pair for the same (155-mm) gun. The first cluster (denoted by white-filled circles) represents the observations on the first day (26 firings over 120 min). Clusters 2, 3, and 4 represent the observations on the second day (which are the same observations of the EW source bearing shown in Fig. 16). Cluster 5 represents the observations on the third day (32 firings over 90 min). The mean and standard deviation for each cluster are calculated and then plotted in Fig. 18(b)—gun A. The corresponding results for the NS source bearing estimates from the NS sensor pair are shown in Fig. 18(a)—gun A. For completeness, the rest of Fig. 18 shows the results for the primaries of other guns (B and C), a mortar firing serial, and an exploding grenade serial. The variability in the bearing estimates is larger when the source direction is near the end-fire direction of the sensor pair axis; for example, compare the results in Figs. 18(a) and 18(b) for grenade. These results are consistent with those for the artillery gun in the first field experiment [see Fig. 14(a.1) for β_{NS} and Fig. 14(c.1) for β_{EW}].

VI. CONCLUSIONS

Locating an impulsive sound source in air requires accurate time-delay measurements for the acoustic wavefront to travel between sensors, accurate survey information for the sensor positions, and knowledge of the effective speed of sound travel in the atmosphere. The variability in source bearing and position estimates is ascribed to the sound propagation medium being variable in both space and time. The variability in the source position estimates may be reduced by temporal averaging (observing many firing events from the same source over a long period of time) and by spatial averaging (observing the same firing event with many widely distributed nodes).

Source bearing errors resulting from atmospheric winds can be reduced by a prudent choice of sensor orientation, which is found to be preferable to adjusting the speed of sound travel to include the wind-speed variation observed in ground wind vector measurements taken in proximity to the sensors.

The apparent bearings from two orthogonal pairs of sensors can be decomposed into the constituent azimuth and elevation angles. Combining the time-delay estimates from two orthogonal pairs of sensors reduces the source direction bias errors caused by vertical refraction of the wavefronts and enables the source azimuth angle to be estimated directly without having to know the effective speed of sound travel.

ACKNOWLEDGMENTS

The authors gratefully acknowledge the technical discussions with their colleagues: Gary Speechley and Ron Wyber. The authors greatly appreciate the field trials support provided by the soldiers of 1 RISTA (Reconnaissance Intelligence Surveillance and Target Acquisition) Regiment, Australian Army and wish to recognize the leadership of their Commanding Officer (Lieutenant Colonel Rik Modderman).

APPENDIX A: SINGLE PAIR OF SENSORS

The source bearing θ is related to the time delay τ by Eq. (3). (All subscripts are dropped for simplicity.) Let $\Delta\theta$ be the error in the source bearing estimate. Denote $E[\cdot]$ as the ensemble average of the quantity in brackets. Then, $E[\Delta\theta]$ and $E[\Delta\theta^2]$ represent the bias error and mean-square error in the source bearing estimate, respectively.

1. Effect of time-delay error

By definition,

$$E[\Delta\theta^n]=\int_{-\infty}^{\infty}\left[\cos^{-1}\left(\frac{c(\tau+\Delta\tau)}{d}\right)-\theta\right]^n \times f_1(\Delta\tau)d\Delta\tau, \quad n=1,2,..., \tag{A1}$$

where $f_1(\Delta\tau)$ is the probability density function (PDF) of the time-delay estimate error $\Delta\tau$. By expanding the arc cosine function in Eq. (A1) as a Taylor series about the true value, and retaining the second-order and the first-order terms, respectively, it can be shown that

$$E[\Delta\theta]\cong-\frac{c}{d\sin\theta}E[\Delta\tau]-\frac{c^2\cos\theta}{2d^2\sin^3\theta}E[\Delta\tau^2], \tag{A2}$$

$$E[\Delta\theta^2]\cong\left(\frac{c}{d\sin\theta}\right)^2E[\Delta\tau^2], \tag{A3}$$

where $E[\Delta\tau]$ and $E[\Delta\tau^2]$ are the bias error and mean-square error of the time-delay estimate, respectively.

2. Effect of sound-speed error

$$E[\Delta\theta^n]=\int_{-\infty}^{\infty}\left[\cos^{-1}\left(\frac{(c+\Delta c)\tau}{d}\right)-\theta\right]^n \times f_2(\Delta c)d\Delta c, \quad n=1,2,..., \tag{A4}$$

where $f_2(\Delta c)$ is the PDF of the sound-speed error Δc.

A second-order approximation of Eq. (A4) gives the bias error in the bearing estimate

$$E[\Delta\theta]\cong-\frac{\tau}{d\sin\theta}E[\Delta c]-\frac{\tau^2\cos\theta}{2d^2\sin^3\theta}E[\Delta c^2], \tag{A5}$$

where $E[\Delta c]$ and $E[\Delta c^2]$ are the bias error and mean-square error of the assumed sound speed, respectively. A first-order approximation of Eq. (A4) gives the mean-square error in the bearing estimate

$$E[\Delta\theta^2]\cong\left(\frac{\tau}{d\sin\theta}\right)^2E[\Delta c^2]. \tag{A6}$$

3. Effect of vertical refraction

When there is vertical refraction, Eq. (3) provides an estimate of the *apparent* bearing β rather than the actual bearing (azimuth angle) of the source θ. This is because $c\tau/d=\cos\theta\cos\phi=\cos\beta$, where ϕ is the vertical refraction

angle or the apparent source elevation angle. The bearing error due to vertical refraction is $\Delta\theta=\beta-\theta$, so

$$E[\Delta\theta^n]=\int_0^{\pi/2}[\cos^{-1}(\cos\theta\cos\phi)-\theta]^n f_3(\phi)d\phi,$$

$$n=1,2,..., \tag{A7}$$

where $f_3(\phi)$ is the PDF of ϕ. The apparent bearing β is a (positively) biased estimator of the actual bearing θ because $\beta>\theta$.

APPENDIX B: TWO ORTHOGONAL PAIRS OF SENSORS

The source bearing θ is related to the time delays τ_{12} and τ_{13} by Eq. (4). (The subscript NS is dropped for simplicity.)

1. Effect of time-delay errors

$$E[\Delta\theta^n]=\int_{-\infty}^{\infty}\int_{-\infty}^{\infty}\left[\tan^{-1}\left(\frac{\tau_{13}+\Delta\tau_{13}}{\tau_{12}+\Delta\tau_{12}}\right)-\theta\right]^n \times f(\Delta\tau_{12},\Delta\tau_{13})d\Delta\tau_{12}d\Delta\tau_{13}, \quad n=1,2,..., \tag{B1}$$

where $f(\Delta\tau_{12},\Delta\tau_{13})$ is the joint PDF of the time-delay estimate errors $\Delta\tau_{12}$ and $\Delta\tau_{13}$.

Using a first-order approximation and assuming that $\Delta\tau_{12}$ and $\Delta\tau_{13}$ are (statistically) independent, zero-mean, and with the same variance $E[\Delta\tau^2]$, it can be shown that

$$E[\Delta\theta^2]\cong\left(\frac{c}{d}\right)^2 E[\Delta\tau^2]. \tag{B2}$$

2. Effect of vertical refraction

Equation (4) provides an estimate of the source azimuth angle θ, even when the acoustic wavefront undergoes vertical refraction. This is because the two sensor pairs are orthogonal and so $c\tau_{12}/d=\cos\theta\cos\phi$, $c\tau_{13}/d=\sin\theta\cos\phi$, where ϕ is the vertical refraction angle; dividing the second equation by the first gives $\tan\theta=\tau_{13}/\tau_{12}$. Thus, vertical refraction does not cause any error in bearing (azimuth angle) estimation using two orthogonal pairs of sensors. However, it may enhance the effects of other sources of errors on bearing estimation. For example, for a given vertical refraction angle ϕ, the mean-square bearing error due to time-delay estimation errors is given by

$$E[\Delta\theta^2]\cong\left(\frac{c}{d\cos\phi}\right)^2 E[\Delta\tau^2], \tag{B3}$$

which increases with ϕ.

[1] L. L. Beranek, "Unsolved military noise problems," J. Acoust. Soc. Am. **24**, 769–772 (1952).
[2] "Artillery Training—General Principles and Practice of Sound Ranging" VI, Obs. Pam. No. 5, Chief of the Imperial General Staff, (UK) War Office (1957).
[3] T. R. Ford, "Sound Ranging," Royal Australian Artillery Corps Training Manual 3, Pam. No. 7, 5–34 (1988).
[4] G. C. Carter, "Time delay estimation for passive sonar signal processing," IEEE Trans. Acoust., Speech, Signal Process. **ASSP-29**, 463–470 (1981).
[5] G. C. Carter, *Coherence and Time Delay Estimation* (IEEE, New York, 1993).
[6] J. C. Hassab, B. W. Guimond, and S. C. Nardone, "Estimation of location and motion parameters of a moving source observed from a linear array," J. Acoust. Soc. Am. **70**, 1054–1061 (1981).
[7] P. Heimdal and F. Bryn, "Passive ranging techniques," in *Signal Processing*, edited by J. W. R. Griffiths, P. L. Stocklin, and C. Van Schooneveld (Academic, New York, 1973), pp. 261–269.
[8] B. G. Ferguson, "Variability in the passive ranging of acoustic sources in air using a wavefront curvature technique," J. Acoust. Soc. Am. **108**, 1535–1544 (2000).
[9] D. J. Torrieri, "Statistical theory of passive location systems," IEEE Trans. Aerosp. Electron. Syst. **AES-20**, 183–198 (1984).
[10] J. E. Piercy, T. F. W. Embleton, and L. C. Sutherland, "Review of noise propagation in the atmosphere," J. Acoust. Soc. Am. **61**, 1403–1418 (1977).
[11] T. F. W. Embleton, "Tutorial on sound propagation outdoors," J. Acoust. Soc. Am. **100**, 31–48 (1996).
[12] D. K. Wilson, "Performance bounds for acoustic direction-of-arrival arrays operating in atmospheric turbulence," J. Acoust. Soc. Am. **103**, 1306–1319 (1998).